Applied Catalysis B: Environmental 111–112 (2012) 200–207

Contents lists available at SciVerse ScienceDirect

Applied Catalysis B: Environmental

journal homepage: www.elsevier.com/locate/apcatb

Core–shell nanostructure electrodes for improved electrocatalytic properties in methanol electrooxidation

Jong-Min Lee[a], Seong-Bae Kim[a], Young-Woo Lee[a], Do-Young Kim[a], Sang-Beom Han[a], Bumwook Roh[b], Inchul Hwang[b], Kyung-Won Park[a,*]

[a] Department of Chemical Engineering, Soongsil University, Seoul 156-743, Republic of Korea
[b] Hyundai Motor Company, Mabuk-Ri, Gyeonggi-Do, Republic of Korea

ARTICLE INFO

Article history:
Received 26 March 2011
Received in revised form
21 September 2011
Accepted 28 September 2011
Available online 6 October 2011

Keywords:
Core–shell
TiN@C
Nanostructure
Support
Methanol electrooxidation

ABSTRACT

TiN@C nanostructure supports consist of TiN as a core prepared at 900 °C in NH_3 and carbon as a shell by heat treatment of the TiN at 900 °C in CH_4 for 1, 3, and 6 h (referred as TiN@C-1 h, TiN@C-3 h, and TiN@C-6 h). The thickness of the carbon shell layers in the TiN@C supports increase with increasing reaction time at 900 °C in CH_4. In particular, the TiN@C-1 h supported Pt catalyst exhibits much improved electrocatalytic properties toward methanol electrooxidation as compared to Pt catalysts on Vulcan XC-72R.

1. Introduction

Direct methanol fuel cells (DMFCs) are excellent power sources for portable and transportation applications because of their relatively high energy density and handling of liquid fuel at low operating temperatures. However, poor methanol oxidation activity at the anode and high cost of noble metal catalysts are major issues for practical development of DMFCs [1–6]. However, the main problem in the DMFCs is to find a catalyst with such an excellent catalytic activity and stability. Accordingly, it has been solved that the addition of second metallic components or supporting materials is an effective way to promote the electrocatalytic activity and stability of Pt catalysts for methanol oxidation.

In general, the requirements of supporting materials are as follows: high conductivity, excellent crystallinity, high surface area, stability, and interaction with catalyst. Recently, carbonaceous materials have received interests as a catalyst support in fuel cell applications due to their high external surface, good electronic conductivity, and large surface to volume ratio [7–16]. Furthermore, transition metal nitrides are hard and wear-resistant with high melting points and good chemical resistance. In particular, titanium nitride (TiN) exhibits several properties such as hardness, chemical stability, and electrical conductivity [17–25].

Herein, we suggest a novel nanostructure support consisting of TiN as a core and carbon as a shell (TiN@C) for methanol electrooxidation. The TiN@C nanostructure support consists of TiN as a core prepared at 900 °C in NH_3 and carbon as a shell by heat treatment of the TiN at 900 °C in CH_4. The particle size and crystal structure of the supports were characterized using transmission electron microscopy (TEM), X-ray diffraction (XRD) method, and Raman spectrometer. The electrochemical properties of the supports were characterized using potentiostat. The electrocatalytic properties of TiN@C supported Pt catalysts were compared to those of conventional carbon supported Pt catalyst.

2. Experimental

2.1. Synthesis of TiN and TiN@C nanostructure supports

The TiO_2 powders (Degussa, P-25) were prepared by heat treatment under NH_3 and CH_4 gas atmosphere. Firstly, the flow rate of N_2 gas was kept for 1 h at 100 mL min^{-1} to get rid of O_2. Subsequently, with NH_3 gas flow rate of 100 mL min^{-1}, the furnace was heated from room temperature to 900 °C at the rate of 5 °C min^{-1} and then maintained at 900 °C for 8 h. After the formation of the TiN as a core in the TiN@C, N_2 gas flow constant to 900 °C for 30 min. To deposit the carbon layers of the TiN@C supports, the TiN samples

* Corresponding author. Tel.: +82 2 820 0613; fax: +82 2 812 5378.
E-mail address: kwpark@ssu.ac.kr (K.-W. Park).

0926-3373/$ – see front matter © 2011 Elsevier B.V. All rights reserved.
doi:10.1016/j.apcatb.2011.09.036

were kept under CH_4 atmosphere at 900 °C for 1, 3, and 6 h, respectively. Finally, the obtained TiN@C supports were allowed to cool down to room temperature under CH_4 atmosphere.

2.2. Preparation of TiN and TiN@C-supported Pt nanoparticle catalyst

For the preparation of TiN and TiN@C supported Pt (20 wt.%) catalysts, the TiN and TiN@C powders were dispersed into de-ionized water and then $H_2PtCl_6{\cdot}6H_2O$ was dissolved in the solution with continuous stirring for 1 h. After the complete dissolution, $NaBH_4$ solution with an excess amount as a reductant was added to the mixture solution and continuously stirred at 25 °C for 2 h. Finally, the resulting precipitate was washed with de-ionized water and dried at 80 °C oven.

2.3. Characterizations

The supports and catalysts were characterized by transmission electron microscopy (TEM) using a Philips CM20T/STEM electron microscope system at 200 kV. The TEM samples were prepared by placing a drop of the catalyst suspension with ethanol on a carbon-coated copper grid. Structural analysis of the samples was carried out using Rigaku diffractometer equipped with a Cu Kα radiation source of $\lambda = 0.15418$ nm with a Ni filter. The tube current was 100 mA with a tube voltage of 40 kV. The 2θ between 20 and 80° was explored at a scan rate of 4° min^{-1}. Raman spectra were recorded on Mirco-Raman spectrometer (Jobin Yvon HR800 UV) using an Ar ion laser with $\lambda = 514.5$ nm.

Electrochemical measurements were carried out using a three electrode cell. A Pt gauze and Ag/AgCl (in saturated KCl) were used as a counter and reference electrode, respectively. The glassy carbon electrode as a working electrode was polished with 1, 0.3, and 0.05 μm Al_2O_3 paste and then washed in deionized water. The catalyst inks were prepared by ultrasonically dispersing the powders in an appropriate amount of Millipore water. The catalyst ink was deposited onto a glassy carbon working electrode (geometrical area of 0.0706 cm^2). After drying in 50 °C oven, the total metal loading of Pt/TiN@C, Pt/TiN, and Pt/C was 120 and 60 μg cm^{-2}, respectively. The solutions of 0.5 M H_2SO_4 and 2 M CH_3OH + 0.5 M H_2SO_4 were continuously stirred and purged with argon gas. The CO-stripping voltammetry was measured using CO-saturated 0.5 M H_2SO_4 solution. To identify electrochemical properties of the catalysts and supports, cyclic voltammetry and chronoamperometry for the catalysts were performed using a potentiostat (Eco Chemie, AUTOLAB) at room temperature. All potentials were reported with respect to Ag/AgCl.

3. Results and discussion

The nanostructure supports were obtained by heating TiN synthesized under CH_4 atmosphere at 900 °C for 1, 3, and 6 h (referred as TiN@C-1 h, TiN@C-3 h, and TiN@C-6 h). As shown in Fig. 1, the XRD patterns of TiN@C-1 h, TiN@C-3 h, and TiN@C-6 h represent the characteristic peaks of (1 1 1) at $2\theta = 36.6°$, (2 0 0) at $2\theta = 42.5°$, (2 2 0) at $2\theta = 61.8°$, (3 1 1) at $2\theta = 74°$, and (2 2 2) at $2\theta = 77.9°$ corresponding to those of typical TiN phase. Also, all the samples represent characteristic peaks at $2\theta = 25.5°$ corresponding to (0 0 2) of graphite-like carbon. With increasing reaction time from 1 to 6 h at 900 °C, the XRD intensities of graphite-like carbon gradually increase suggesting that the degree of crystallization of the carbon increases.

Fig. 2 shows TEM images of the nanostructure supports of TiN@C-1 h, TiN@C-3 h, and TiN@C-6 h. In all the nanostructure support, carbon layers surround the TiN nanoparticles as a core as a shell (Fig. 2(a–c)). The spacing distance of 0.214 nm corresponds to

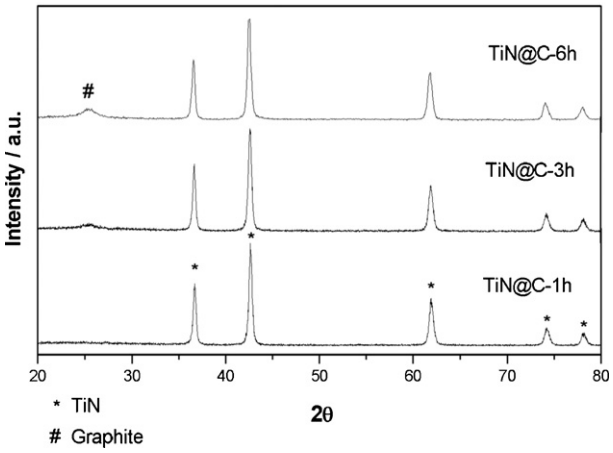

Fig. 1. XRD patterns of the samples obtained by heat treatment under NH_3 and CH_4 atmosphere at 900 °C.

(2 0 0) plane of crystalline TiN with well-developed lattice structure (Fig. 2(d–f)). Furthermore, the carbon shell in the nanostructure supports shows graphite-like carbon structure with the spacing distance of 0.34 nm, which the shell thickness of carbon layer increases with increasing reaction time at 700 °C. Also, as shown in Fig. 2(d–f), the *d*-spacing of the graphitic layer is 0.34 nm, which is similar to that of 0.335 nm corresponding to typical graphite. The thickness of carbon shell layer in TiN@C-1 h, TiN@C-3 h, and TiN@C-6 h is ~2.0, 4.5, and 14.0 nm, respectively. Since carbon layers are formed by means of the heat treatment process during any reaction time, the shell thickness of the TiN@C nanoparticles increases with increasing graphitization with increasing reaction times. The formation of TiN@C core–shell nanostructures may take place as Eqs. (1) and (2):

$$6TiO_2(s) + 8NH_3(g) \rightarrow 6TiN(s) + 12H_2O(g) + N_2(g) \quad (1)$$

$$(2)\ TiN + CH_4 \rightarrow TiN + C_{ad} + 2H_2 \rightarrow TiN@C$$

According to the formation mechanism of the TiN@C core–shell nanostructures, the thickness of carbon layers can be controlled as a function of reaction times. Thus, it is expected that the surface of the TiN nanoparticles is fully covered with a graphite-like carbon film of various thicknesses, which may result in such an excellent interaction and contact between titanium nitride and carbon.

The nature of the carbon present in the TiN@C was investigated by Raman spectroscopy and the results are shown in Fig. 3. All the spectra indicate two peaks around 1341 and 1596 cm^{-1}. The Raman-active E2g mode at ~1596 cm^{-1} is characteristic of graphitic sheets. The well-defined G-band for all the samples confirms the presence of sp2 carbon-type structures within the carbonaceous wall of TiN@C. The D-band at ~1341 cm^{-1} can be attributed to the presence of defects within the hexagonal graphitic structure. Since the intensities of the G-bands are comparable to those of the D-bands, the samples have some degree of atomic-scale ordering. Compared with the spectra of pure graphite crystals (1575 cm^{-1}), the higher shift of the G-band in the spectra suggests some structural imperfections of the carbon shells [26].

Fig. 4 shows the XRD patterns of Pt catalysts supported by TiN@C-1 h, TiN@C-3 h, and TiN@C-6 h (referred as Pt/TiN@C-1 h, Pt/TiN@C-3 h, and Pt/TiN@C-6 h, respectively) as compared to Vulcan XC-72R supported Pt catalyst (Pt/Vulcan XC-72R). As can be seen in the XRD patterns of all the supported catalysts, the main diffraction peaks $2\theta = 39.7°$, 46.2° and 67.4°, which associated with (1 1 1), (2 0 0) and (2 2 0) planes of face-centered-cubic structure of Pt, respectively. Moreover, as already indicated in Fig. 1, the nanostructure supported catalysts exhibits the XRD patterns corresponding to crystalline TiN and graphite-like carbon for TiN@C-1 h, TiN@C-3 h, and TiN@C-6 h. On the other hand, the XRD patterns

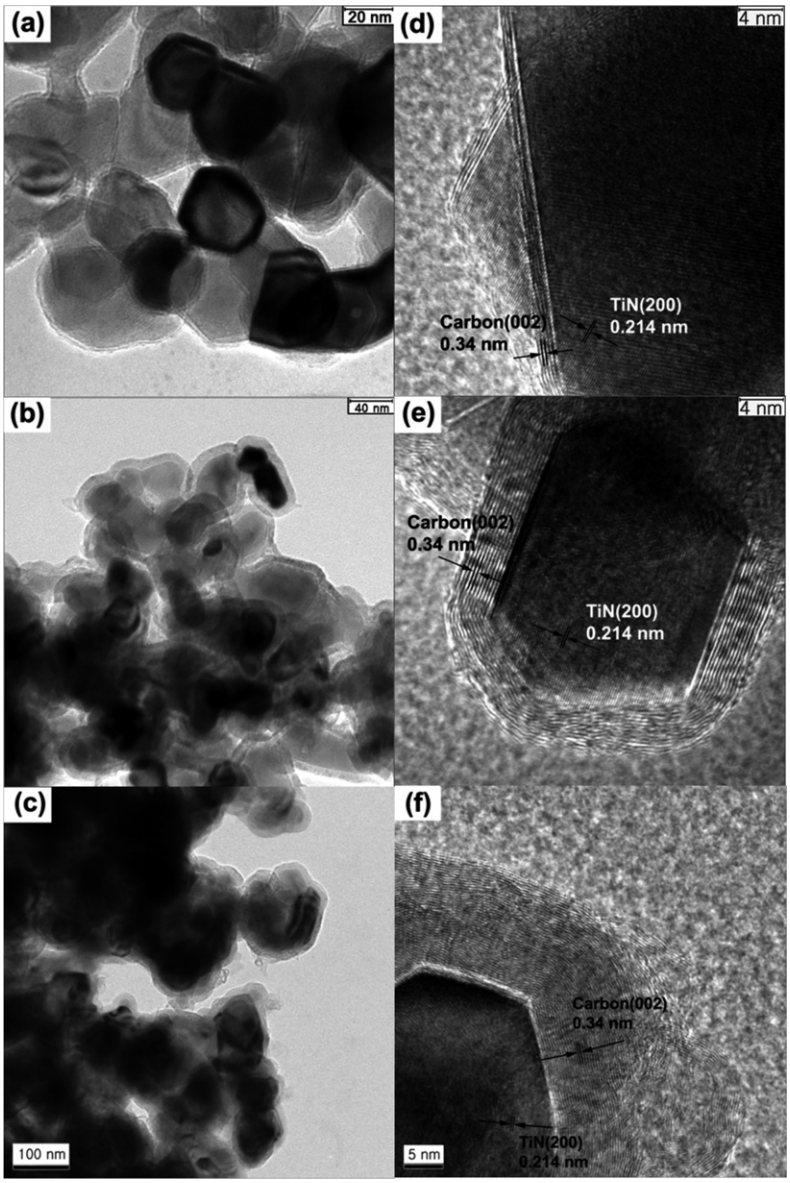

Fig. 2. TEM and HR-TEM images of TiN@C-1 h [(a), (d)], TiN@C-3 h [(b), (e)], and TiN@C-6 h [(c), (f)].

of Pt/Vulcan XC-72R consist of characteristic peaks of Pt catalyst and amorphous carbon support. Fig. 5(a–d) shows TEM images of Pt catalysts deposited on Vulcan XC-72R, TiN@C-1 h, TiN@C-3 h, and TiN@C-6 h, respectively. The Pt/TiN@C showed homogeneously

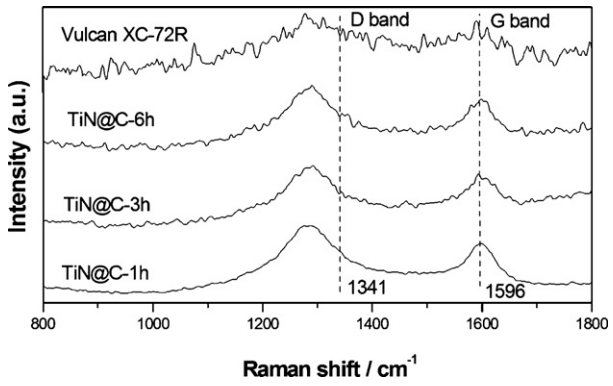

Fig. 3. Raman spectra of TiN@C core–shell nanostructure supports as compared to Vulcan XC-72R.

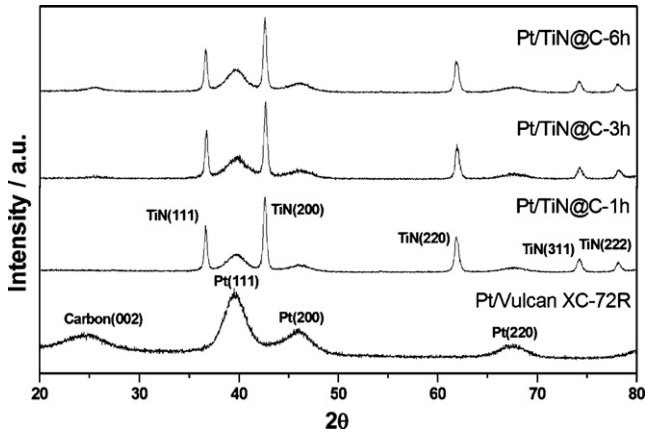

Fig. 4. XRD patterns of Vulcan XC-72R, TiN@C-1 h, TiN@C-3 h, and TiN@C-6 h supported Pt catalysts.

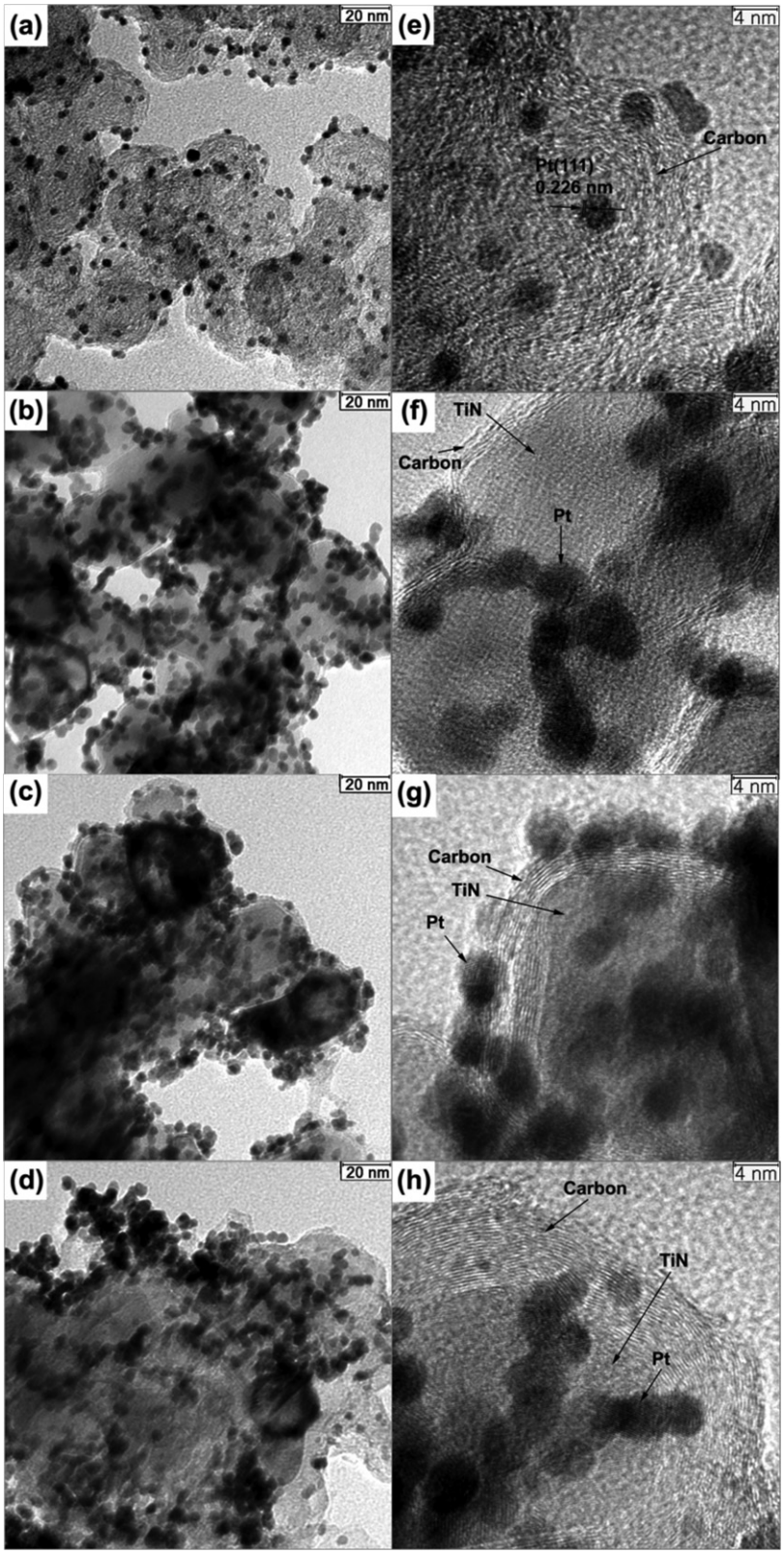

Fig. 5. TEM and HR-TEM images of Pt/Vulcan XC-72R[(a), (e)], Pt/TiN@C-1 h [(b), (f)], Pt/TiN@C-3 h [(c), (g)], and Pt/TiN@C-6 h [(d), (h)].

dispersed Pt nanoparticles of ~4 nm in average size on the TiN@C supports and those of ~3 nm on the Vulcan XC-72R. Especially, from the HRTEM image of Fig. 5(f–h), Pt nanocatalysts are fairly well deposited on TiN@C supports. It is likely that the configuration could affect the stability of catalytic reaction and interaction between catalyst and support.

Compared to electrochemical properties of Pt/Vulcan XC-72R, cyclic voltammograms (CVs) of the Pt/TiN@C-1 h, Pt/TiN@C-3 h, and Pt/TiN@C-6 h are represented in Fig. 6, indicating the presence of polycrystalline Pt. The peaks for the adsorption/desorption of hydrogen and preoxidation/reduction on the Pt surface in H_2SO_4 electrolyte are clearly shown. The electrochemical properties for

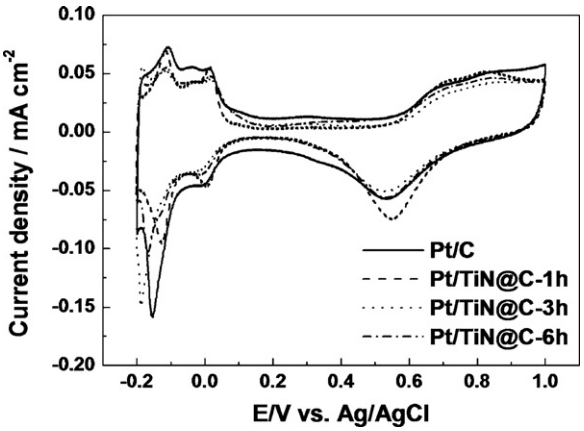

Fig. 6. CVs of Pt/Vulcan XC-72R and Pt/TiN@C in 0.5 M H_2SO_4.

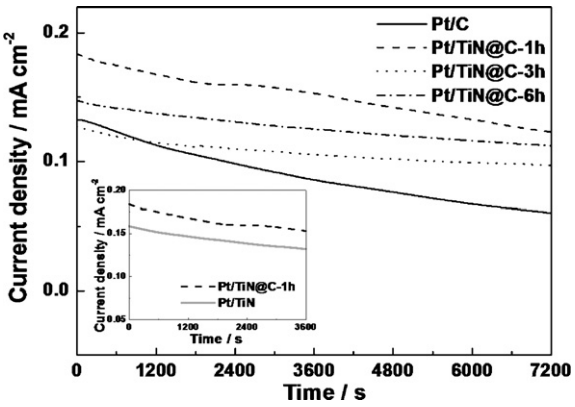

Fig. 8. Plots of oxidation current versus time of supported Pt catalysts measured at 0.4 V for 7200s in 2 M CH_3OH + 0.5 M H_2SO_4. The inset indicates the performance comparison of Pt/TiN@C-1 h and Pt/TiN.

the core–shell nanostructure supported catalysts may be due to an improved electronic conductivity and stability in acid solution of the nanostructured support and its interaction with catalysts. Furthermore, electrocatalytic properties for methanol electrooxidation of Pt/TiN@C-1 h, Pt/TiN@C-3 h, Pt/TiN@C-6 h, and Pt/Vulcan XC-72R were investigated by CVs in 0.5 M H_2SO_4 + 2 M CH_3OH. The area-normalized currents for methanol electrooxidation were obtained as shown in Fig. 7(a). The methanol electrooxidation current was normalized by the electrochemical surface area of the active sites assuming charge density of 210 $\mu C\,cm^{-2}$ of hydrogen adsorption on polycrystalline Pt electrode. Therefore, the area-normalized current represents the intrinsic activity of the active sites in the catalysts. In the methanol electrooxidation, the first anodic peak is usually indicated to the oxidation of methanol molecules on the electrode surface, while the backward anodic peak is generally attributed to the continuous oxidation of incompletely oxidized carbonaceous intermediates accumulated on the catalyst surface during the forward scan, such as CO_{ads}, $COOH_{ads}$, and COH_{ads} [27,28]. The ratio of the forward anodic peak current density (I_f) to the reverse anodic peak current density (I_b), i.e., I_f/I_b, can be used to describe the catalyst tolerance to carbonaceous species accumulation. The low I_f/I_b ratio indicates poor oxidation of methanol to carbon dioxide during the forward anodic scan and excessive accumulation of carbonaceous residues on the catalyst surface. On the other hand, the high I_f/I_b ratio indicates excellent oxidation of methanol during the reverse anodic scan and less accumulation of residues on the catalyst [29–31]. The high I_f/I_b values on Pt/TiN@C-1 h, Pt/TiN@C-3 h, and Pt/TiN@C-6 h implicates that methanol molecules can be more effectively oxidized on Pt/TiN@C catalysts during the forward potential scan, generation relatively less poisoning species as compared to Pt/Vulcan XC-72R. As shown in Fig. 7(a), the current density at 0.4 V for Pt/TiN@C-1 h is much higher than those for Pt/TiN@C-3 h, Pt/TiN@C-6 h, and Pt/Vulcan XC-72R. Furthermore, the Pt/TiN@C-1 h (0.184 mA cm^{-2}) appears 1.16 times higher current density in comparison with Pt/TiN (0.159 mA cm^{-2}) at 0.4 V. This means that TiN@C-1 h support exhibits optimized electrochemical properties due to interaction of TiN support and improved conductivity by carbon shell. Fig. 7(b) shows curve of mass–current density of the supported catalysts in 0.5 M H_2SO_4 + 2.0 M CH_3OH. The maximum mass current density of methanol electrooxidation of Pt/TiN@C-1 h (0.913 A mg_{Pt}^{-1}) is higher than those of Pt/TiN@C-3 h (0.805 A mg_{Pt}^{-1}), Pt/TiN@C-6 h (0.803 A mg_{Pt}^{-1}), and Pt/Vulcan XC-72R (0.795 A mg_{Pt}^{-1}).

Fig. 8 shows curves of current density versus time of the supported catalysts at 0.4 V for 7200 s in 0.5 M H_2SO_4 + 2 M CH_3OH. The Pt/TiN@C-1 h maintains much higher current and the final current density is 0.123 mA cm^{-2} in comparison with Pt/TiN@C-3 h, Pt/TiN@C-6 h, and Pt/Vulcan XC-72R (0.097, 0.113, and 0.061 mA cm^{-2}, respectively). Furthermore, the Pt/TiN@C-1 h (0.184 mA cm^{-2}) appears 1.16 times higher current density in comparison with Pt/TiN (0.159 mA cm^{-2}) at 0.4 V as indicated in the inset of Fig. 8. This means that enhanced electrochemical properties of Pt catalyst on TiN@C-1 h support may be due to strong interaction of TiN support and improved conductivity of monolayer carbon shell. Since the change of size and morphology for catalysts before and after durability test could affect the whole activity, their size distribution and shape should be observed and

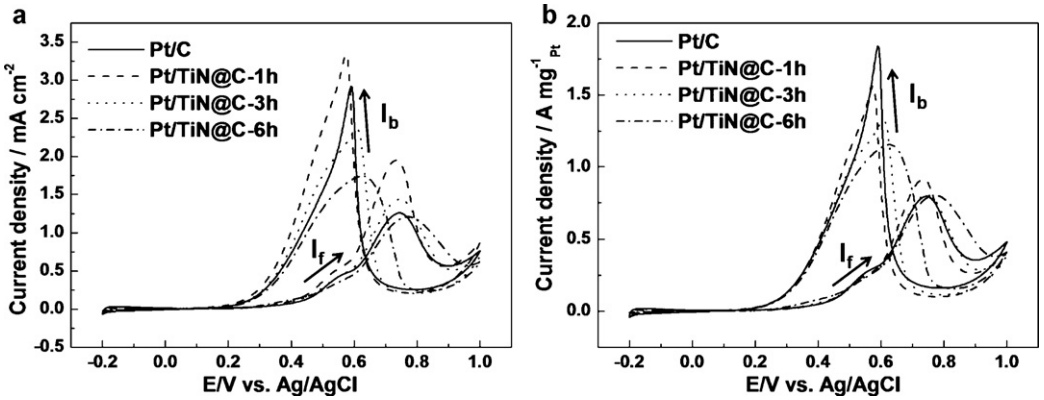

Fig. 7. Cyclic voltammograms (CVs) of supported Pt catalysts measured in 2 M CH_3OH + 0.5 M H_2SO_4 with a scan rate of 50 mV s^{-1} at 25 °C. The electrochemical data were normalized by (a) electrochemical active surface areas and (b) amount of loading of catalysts, respectively.

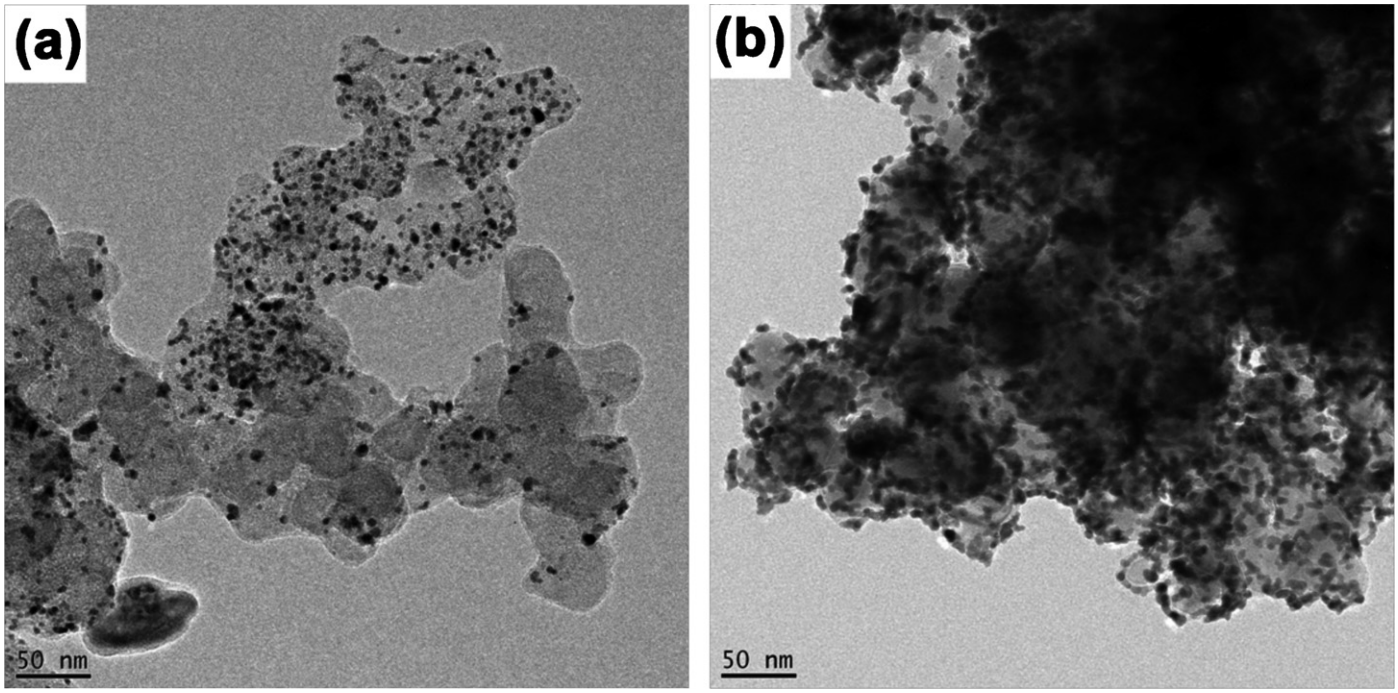

Fig. 9. TEM images of (a) Pt/Vulcan XC-72R and (b) Pt/TiN@C-1 h after the methanol oxidation test at 0.4 V in 2 M CH_3OH + 0.5 M H_2SO_4.

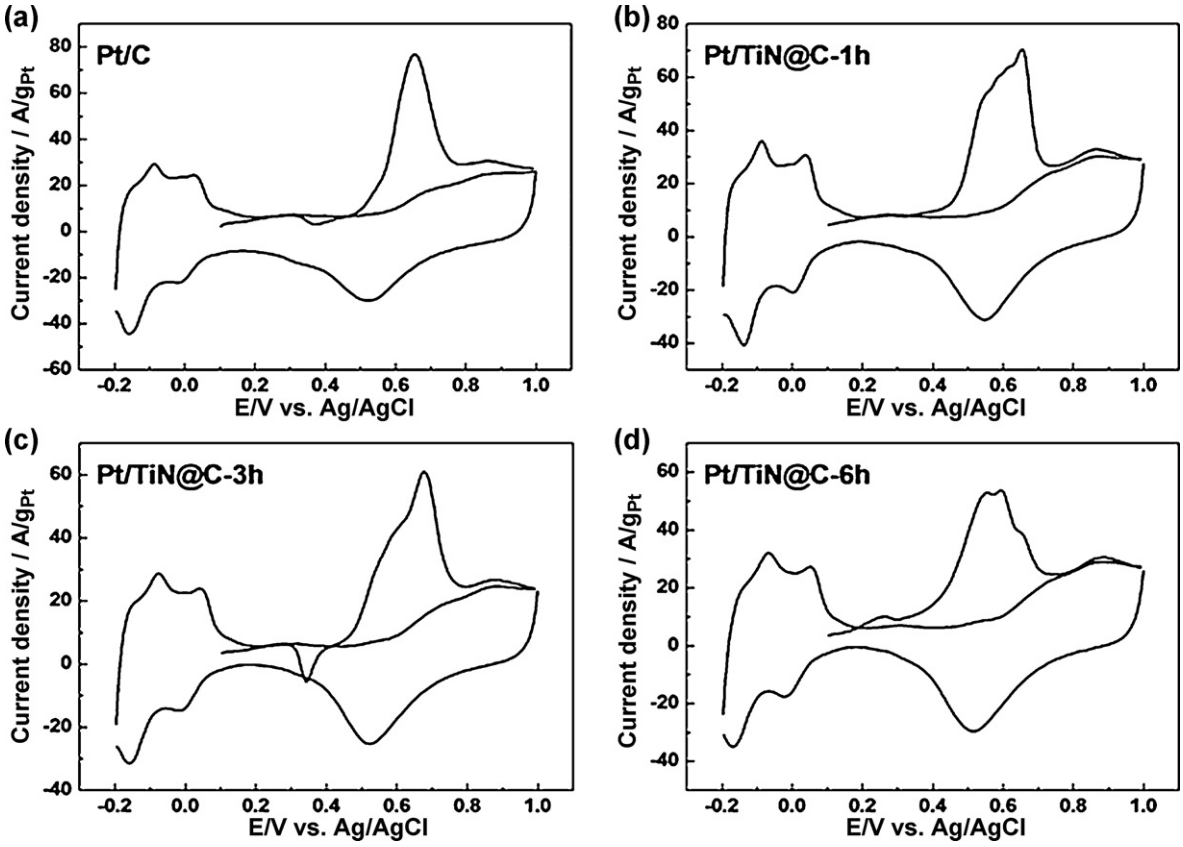

Fig. 10. CO-stripping voltammograms of (a) Pt/C, (b) Pt/TiN@C-1 h, (c) Pt/TiN@C-3 h, and (d) Pt/TiN@C-6 h catalysts in 0.5 M H_2SO_4 solution.

compared (Fig. 9). The Pt/TiN@C-1 h shows a slight reduction of size and nearly maintained morphology after the durability test, retaining such an improved electrocatalytic activity. In contrast, after the durability test, the Pt/Vulcan XC-72R exhibits non-uniform size distribution resulting in deteriorated catalytic activity. To characterize CO-tolerance of the catalysts, CO-stripping voltammetry was performed as shown in Fig. 10. The Pt/TiN@C catalysts exhibit much lower on-set potential toward CO-oxidation than the Pt/C. This suggests that the CO-tolerance of the Pt/TiN@C might result in superior electrocatalytic activity for methanol electrooxidation to the Pt/C.

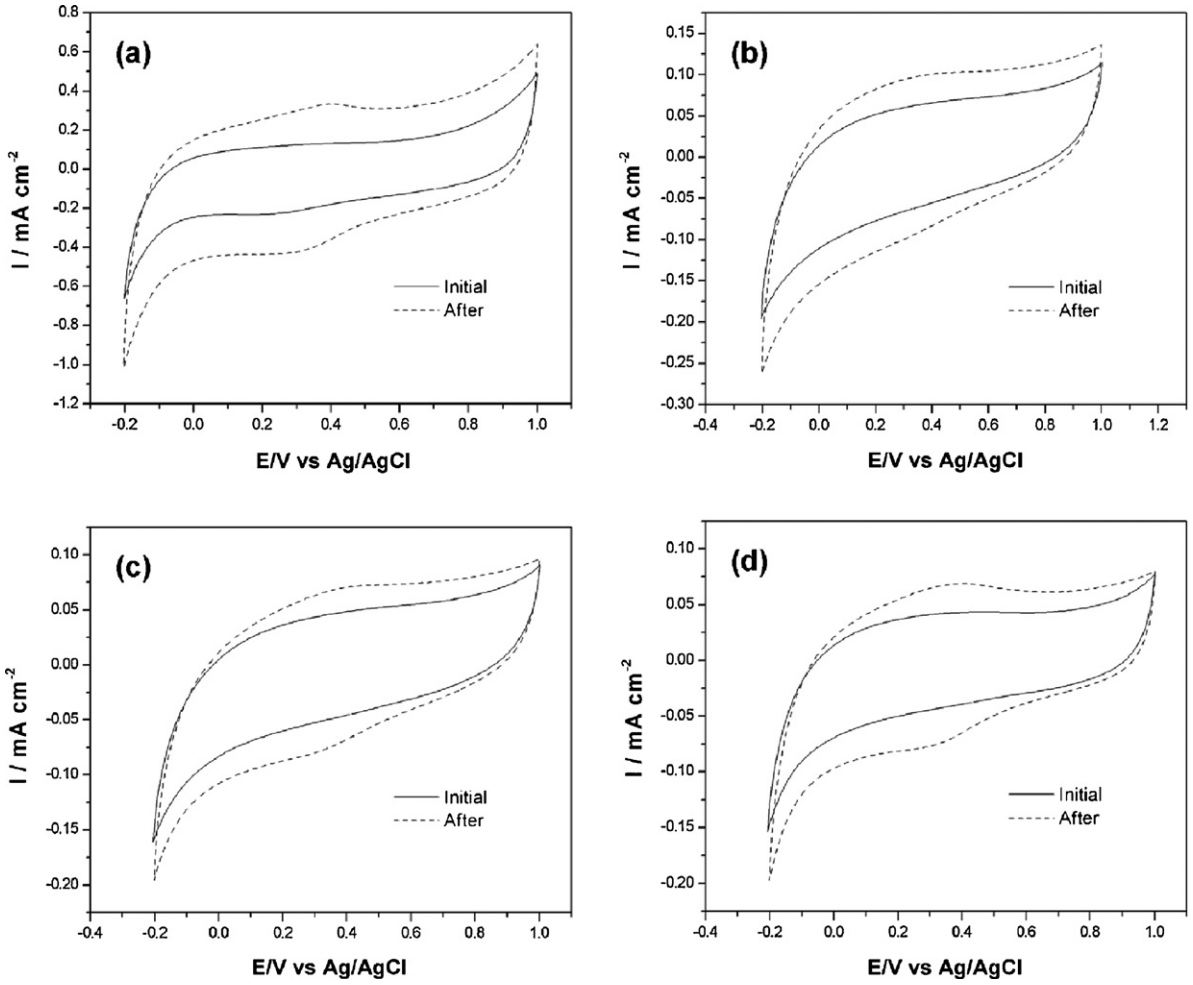

Fig. 11. CVs of (a) Vulcan XC-72R, (b) TiN@C-1 h, (c) TiN@C-3 h, and (d) TiN@C-6 h supports measured before and after 100 cycling between −0.2 and 1.2 V in 0.5 M H_2SO_4.

The CVs of the supports (TiN@C-1 h, TiN@C-3 h, TiN@C-6 h, and Vulcan XC-72R) were measured before and after 100 cycling between −0.2 and 1.2 V as shown in Fig. 11. The variation of area of electrochemical characteristic curves indicates a criterion of stability of supports. In other words, the increased area difference before and after cycling means deteriorated stability of supports due to remarkable changes of surface or chemical states. In the case of the TiN@C-1 h, TiN@C-3 h, and TiN@C-6 h, the ratio of the area change was 1.39, 1.29, and 1.38 in comparison with 1.86 for the Vulcan XC-72R. The smaller area ratio of the TiN@C supports than the Vulcan XC-72R indicates an excellent stability such as corrosion resistance of the core–shell supports in the potential range of fuel cells in comparison with conventional carbon support. Thus, the electrochemical stability of the Pt/TiN@C may be attributed to corrosion resistance of the TiN@C compared to the Vulcan XC-72R.

4. Conclusions

The nanostructure supports consisting of TiN as a core and carbon as a shell have been successfully formed by heating process under CH_4 atmosphere. The carbon layers in the core–shell nanostructures are controlled as a function of reaction temperature. The core–shell nanostructure supported Pt catalysts show improved catalytic activity and stability for methanol electrooxidation compared to those of conventional carbon supported Pt catalyst. The enhanced catalytic properties of the nanostructure supported Pt catalysts may be due to core–shell nanostructure support.

Acknowledgments

This work was supported by Korea Energy Management Corporation (2008-N-FC12-J-01-3-150), Korea Industrial Technology Foundation through the Human Resource Training Project for Strategic Technology, and the Manpower Development Program (20104010100610) for Energy & Resources, the Ministry of Knowledge and Economy.

References

[1] O.A. Petrii, J. Solid State Electrochem. 12 (2008) 609–642.
[2] D.-H. Lim, W.-D. Lee, D.-H. Choi, H.-I. Lee, App. Catal. B: Environ. 94 (2010) 84–96.
[3] T. Kawaguchi, W. Sugimoto, Y. Murakami, Y. Takasu, J. Catal. 229 (2005) 176–184.
[4] B. Yang, Q. Lu, Y. Wang, L. Zhuang, J. Lu, P. Liu, J. Wang, R. Wang, Chem. Mater. 15 (2003) 3552–3557.
[5] V. Selvaraj, M. Alagar, Electrochem. Commun. 9 (2007) 1145–1153.
[6] G.A. Camara, E.A. Ticianelli, S. Mukerjee, S.J. Lee, J. McBreen, J. Electrochem. Soc. 149 (2002) A748–A753.
[7] Y. Gogotsi (Ed.), Carbon Nanomaterials, 1st edition, Taylor & Francis, London, 2006.
[8] B. Fang, J.H. Kim, M. Kim, J.S. Yu, Chem. Mater. 21 (2009) 789–796.
[9] H. Liu, C. Song, L. Zhang, J. Zhang, H. Wang, D.P. Wilkinson, J. Power Sources 155 (2006) 95–110.
[10] S.H. Joo, S.J. Choi, I. Oh, J. Kwak, Z. Liu, O. Terasaki, R. Ryoo, Nature 412 (2001) 169–171.

[11] J.S. Yu, S. Kang, S.B. Yoon, G.S. Chai, J. Am. Chem. Soc. 124 (2002) 9382–9383.
[12] S. Iijima, Nature 354 (1991) 56–57.
[13] H.T. Zheng, Y.L. Li, S.X. Chen, P.K. Shen, J. Power Sources 163 (2006) 371–375.
[14] S.X. Chen, X. Zhang, P.K. Shen, Elecrochem. Commun. 8 (2006) 713–719.
[15] F.Y. Xie, Z.Q. Tian, H. Meng, P.K. Shen, J. Power Souces 141 (2005) 211–215.
[16] Y.Y. Song, Y. Li, X.H. Xia, Electrochem. Commun. 9 (2007) 201–205.
[17] R.L. Fleischer, J. Met. 37 (1985) 16–20.
[18] X.H. Jin, L. Gao, J.G. Li, S. Zheng, J. Am. Ceram. Soc. 87 (2004) 162–165.
[19] J. Musil, Surf. Coat. Technol. 125 (2000) 322–330.
[20] Y. Qiu, L. Gao, J. Phys. Chem. B 109 (2005) 19732–19740.
[21] S. Kaskel, K. Schlichte, T. Kratzke, J. Mol. Catal. A: Chem. 208 (2004) 291–298.
[22] Y.J. Lee, Mater. Lett. 59 (2005) 615–617.
[23] S. Kaskel, K. Schlichte, G. Chaplais, M.J. Khanna, J. Mater. Chem. 13 (2003) 1496–1499.
[24] M.A. Centeno, I. Carrizosa, J.A. Odriozola, Appl. Catal. A: Gen. 246 (2003) 365–372.
[25] H. Zhai, L. Jianbao, Y. Chen, B. Zhang, J. Mater. Chem. 11 (2001) 1092–1095.
[26] L.W. Zhang, H.B. Fu, Y.F. Zhu, Adv. Funct. Mater. 18 (2008) 2180–2189.
[27] Y.X. Chen, A. Miki, S. Ye, H. Sakai, M. Osawa, J. Am. Chem. Soc. 125 (2003) 3680–3681.
[28] W.F. Lin, J.T. Wang, R.F. Savinell, J. Electrochem. Soc. 144 (1997) 1917–1922.
[29] C. Xu, L. Wang, R. Wang, K. Wang, Y. Zhang, F. Tian, Y. Ding, Adv. Mater. 21 (2009) 2165–2169.
[30] C.H. Yen, K. Shimizu, Y.Y. Lin, F. Bailey, I.F. Cheng, C.M. Wai, Energy Fuels 21 (2007) 2268–2271.
[31] Y. Gu, W. Wong, Langmuir 22 (2006) 11447–11452.